Table of Contents

S1: Materials and methods:

All reagents were obtained from commercial sources and used without further purification, unless otherwise noted.

^{1}H NMR and ^{13}C NMR spectra were recorded on a Bruker Advance III 400 and 500 MHz instruments. Chemical shifts for ^{1}H NMR spectra are reported in ppm (δ, relative to TMS) using DMSO residual peak (δ = 2.50 ppm) in DMSO-d_6 as an internal standard and for ^{13}C NMR spectra solvent peaks at 39.52 ppm.

Powder X-ray diffraction (PXRD) measurements were carried out at room temperature on a PANalytical X'Pert PRO diffractometer 45 kV, 40 mA for Cu $K\alpha$ (λ = 1.5418 Å), with a scan speed of 1.0° min^{-1} and a step size of 0.02° in 2θ. Variable Temperature Powder X-ray Diffraction (VT-PXRD) measurements were collected on a PANalytical X'Pert Pro MPD X-ray diffractometer equipped with an Anton-Parr CHC+ variable temperature stage. Measurements were collected at 45 kV, 40 mA for Cu $K\alpha$ (λ = 1.5418 Å) with a scan speed of 1.0° min^{-1} and a step size of 0.02° in 2θ. Samples were placed under vacuum during analysis and analysis and the sample was held at the designated temperatures for at least 15 minutes between each scan.

High resolution dynamic thermogravimetric analysis (TGA) were performed under a continuous N_2 flow and recorded on a TA Instruments hi-res TGA Q500 thermogravimetric analyzer with a heating rate of 1°C per minute.

Fourier-transform Infrared (FT-IR) spectra (4000 – 600 cm^{-1}) were recorded on a Thermo Scientific Nicolet 6700 apparatus.

Low pressure gas adsorption studies of the MOFs were conducted on a fully automated micropore gas analyzer Autosorb-IC (Quantachrome Instruments) at relative pressures up to 1 atm. The temperature was controlled using a cryocooler system (cryogen-free) capable of temperature control from 20 to 320 K.

Low-pressure gas sorption measurements were performed on a fully automated micropore gas analyzer Autosorb-IC (Quantachrome Instruments) at relative pressures up to 1 atm. Single-crystal X-ray diffraction data were collected using an X8 Prospector APEX2 CCD diffractometer (Cu $K\alpha$ λ = 1.54178 Å).

The electrochemical measurements were performed on a Bio-Logic VMP3 potentiostat in both 3-electrode and 2-electrode configurations using 1 M H_2SO_4 as electrolyte at room temperature. In 3-electrode measurements, the MOF material was mixed with carbon black and polyvinylidene fluoride (PVDF) with a weight ratio of 8:1:1 in N-methyl pyrrolidone (NMP) to form a homogeneous ink, which was then drop-casted onto a carbon cloth electrode. After drying in a vacuum oven for overnight, the carbon cloth with active material on it was then used as the working electrode. A Ag/AgCl electrode and a Pt wire were used as the reference and counter electrode, respectively. For 2-electrode measurement, two pieces of the as-fabricated carbon cloth electrodes with almost the same mass loading were used as the positive and negative electrodes respectively with a porous polymer membrane (Celgrad 3501) as the separator to assemble a coin cell. The capacitance (C, F·g^{-1}) reported in this work was calculated from CV curves:

$$C = \frac{\int i_{cathodic}\, dV}{m\upsilon\Delta V}, \qquad (1)$$

where i (mA) is the current, v (mV·s^{-1}) the scan rate, m (g) the mass of the active materials on the single electrodes, and V (V) the potential window.

The energy density (E, Wh·kg^{-1}) and power density (P, W·kg^{-1}) were calculated from the GCD curves:

$$E = \frac{i\int V\, dt}{M \times 3.6} \quad \text{and} \qquad (2)$$

$$P = \frac{E}{t} \times 3600, \qquad (3)$$

where i, (A) is the current, V (V) the cell voltage window, t (s) the discharge time, and M (g) the mass of the active materials on both the positive and negative electrodes.

S2: Synthesis of ligands and MOFs:

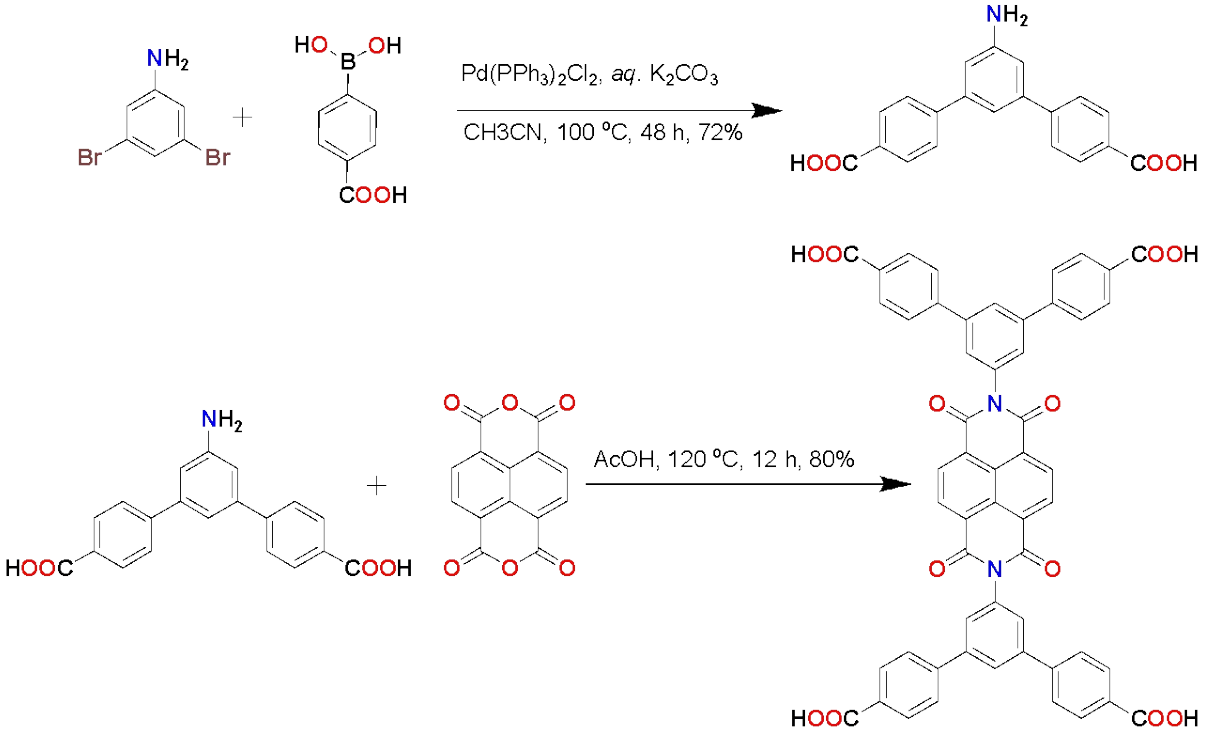

Figure S1: Scheme for synthesis of the ligands from the starting material.

Preparation of aniline-3,5-dibenzoic acid:

250 mL Schlenk flask was charged with 3,5-dibromoaniline (2.2 g, 1 Eq, 8.8 mmol) and 4-boronobenzoic acid (3.2 g, 2.2 Eq, 19 mmol) and evacuated/backfilled with argon. Acetonitrile (40 mL) followed by 2N K_2CO_3 (9.7 g, 35 mL, 8.0 Eq, 70 mmol) were added to the mixture and then solution was bubbled with argon for 1h. To this Pd(PPh$_3$)Cl$_2$ (0.37 g, 6 mol%, 0.53 mmol) was added, flask was argonated, sealed and placed in preheated to 100°C oil bath for 48h. Cooled to room temperature, diluted with water (200 ml), filtered through celite and washed thoroughly with water. The filtrate was acidified to pH ~3 with 2 N HCl (effervescence!), the precipitate was collected by filtration, washed with water, followed by hexane, dried briefly on air, then at high vacuum at 50°C overnight to give aniline-3,5 dibenzoic acid (2.80 g, 96%) as off-white powder.

^{1}H NMR (500 MHz, DMSO-d_6) δ 12.92 (s, 2H), 8.02 (d, J = 8.2 Hz, 4H), 7.79 (d, J = 8.2 Hz, 4H), 7.20 (s, 1H), 6.99 (s, 2H), 5.67 (s, 2H) ppm.

^{13}C NMR (126 MHz, DMSO) δ 167.2, 149.0, 144.9, 140.6, 129.9, 129.6, 126.8, 114.1, 112.7 ppm.

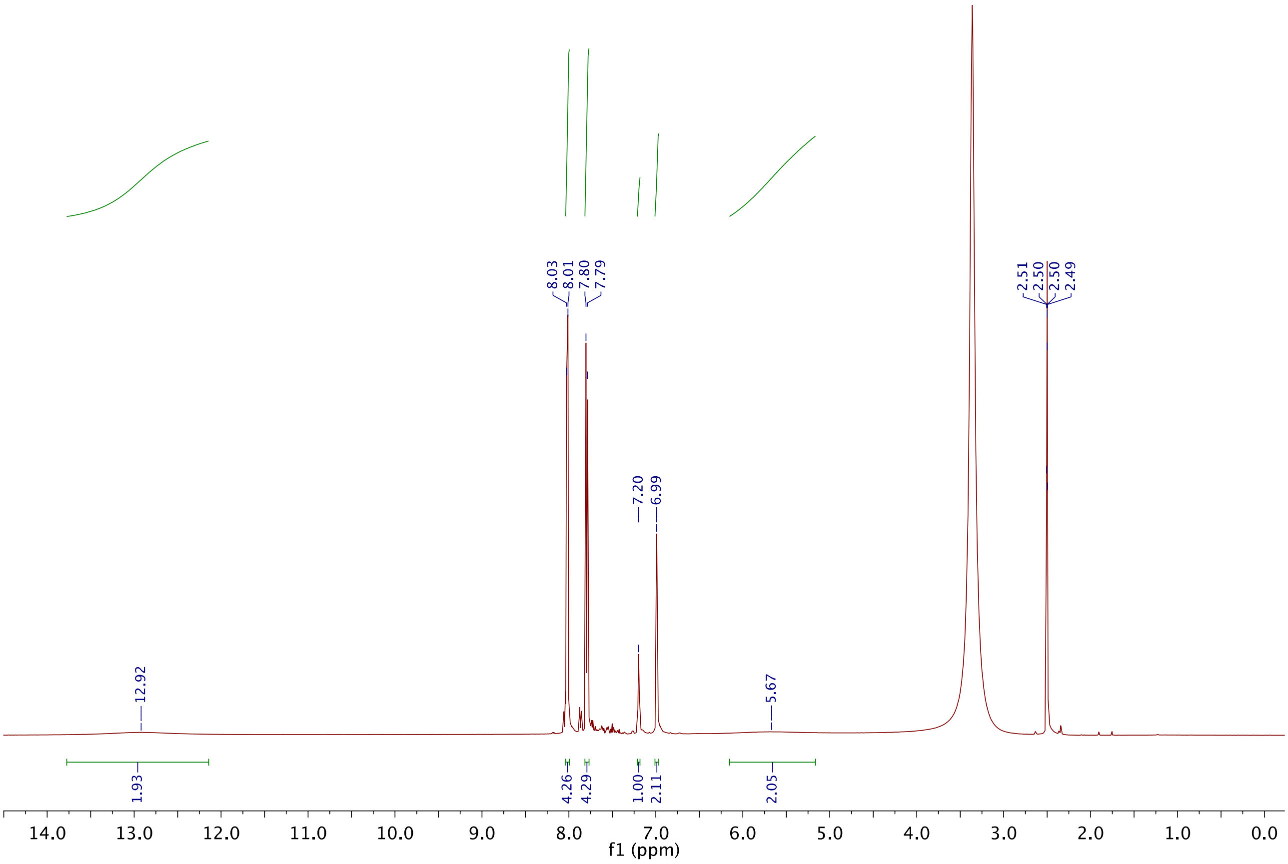

Figure S2: ^{1}H NMR spectra of aniline-3,5 dibenzoic acid (500 mHz, DMSO-d_6).

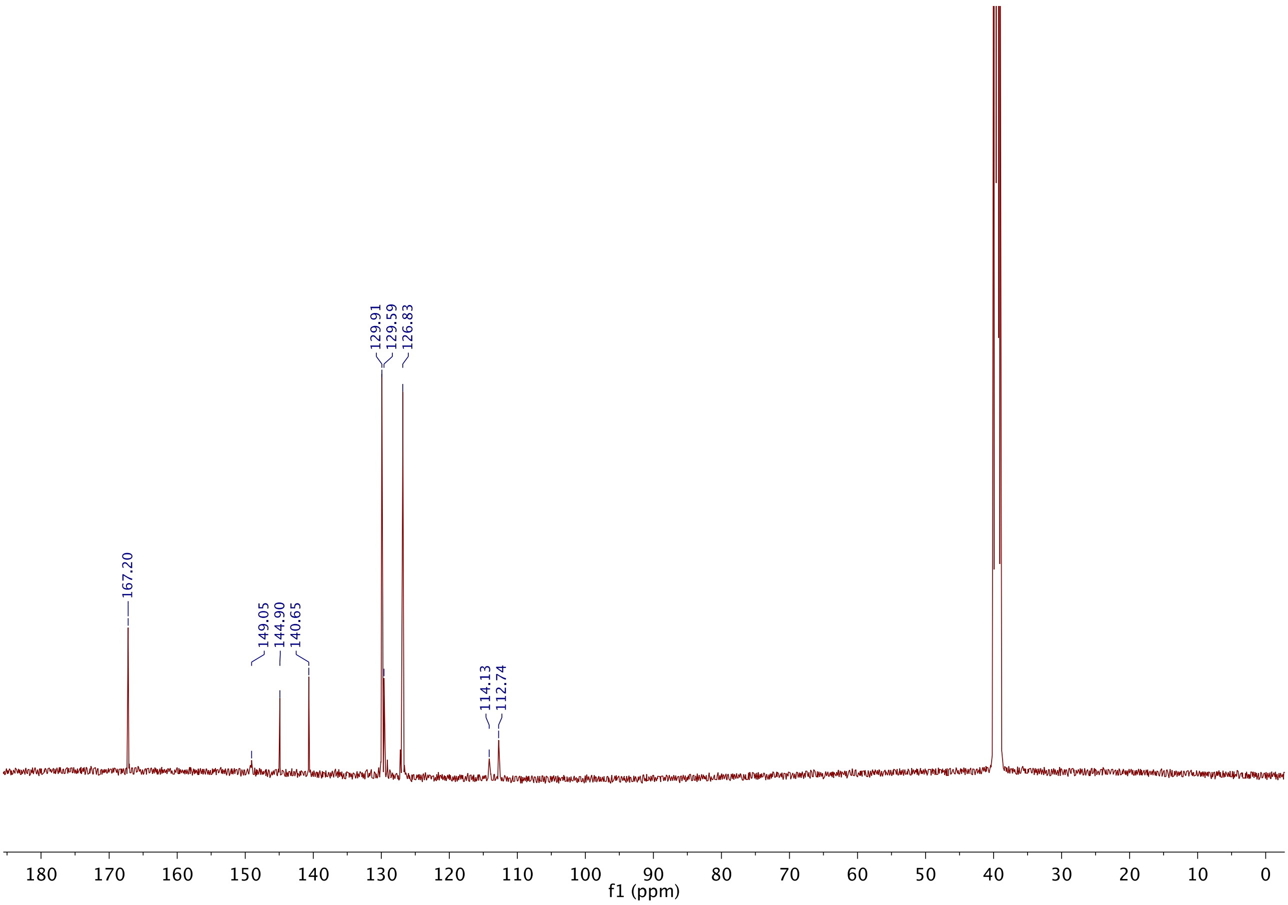

Figure S3: ^{13}C NMR spectra of aniline-3,5 dibenzoic acid (500 mHz, DMSO-d_6).

Preparation of N,N'-bis(terphenyl-4,4''-dicarboxylic acid) naphthalenediimide (H_4BTD-NDI): 1,4,5,8-tetracarboxydianhydride (0.268 g, 1.0 mmol) was taken into a 250 mL round bottomed flask and suspended in 25 mL acetic acid. The mixture was stirred for 10 min. To this solution, anilene-3,5-dibenzoicacid (0.698 g, 2.2 mmol) was added and the solution allowed reflux for 12h. The reaction was allowed to cool to room temperature and water (90 ml) was added to precipitate the product. The product was collected by filtration washed with ethanol and dried in vacuum to yield 2.4 g of off-white solid (isolated yield = 2.4 g, 77%). The compound was recrystallized from DMF as an off-yellow materials (isolated yield = 2.1 g, 67%).

^{1}H NMR (400 MHz, DMSO-*d*$_6$) *δ* 12.44 (s, 4H), 8.76 (s, 4H), 8.19 (s, 2H), 8.06 (d, *J* = 8.2 Hz, 8H), 7.96 (d, *J* = 1.6 Hz, 4H), 7.92 (d, *J* = 8.2 Hz, 8H).

^{13}C NMR (101 MHz, DMSO) *δ* 167.4, 163.0, 142.6, 140.8, 137.1, 131.4, 130.6, 130.0, 127.3, 127.0, 126.9, 126.6, 125.4.

HR-MS (ESI, [M-H]$^-$): calcd for $[C_{54}H_{29}N_2O_{12}]^-$: 897.17260; found: 897.17424.

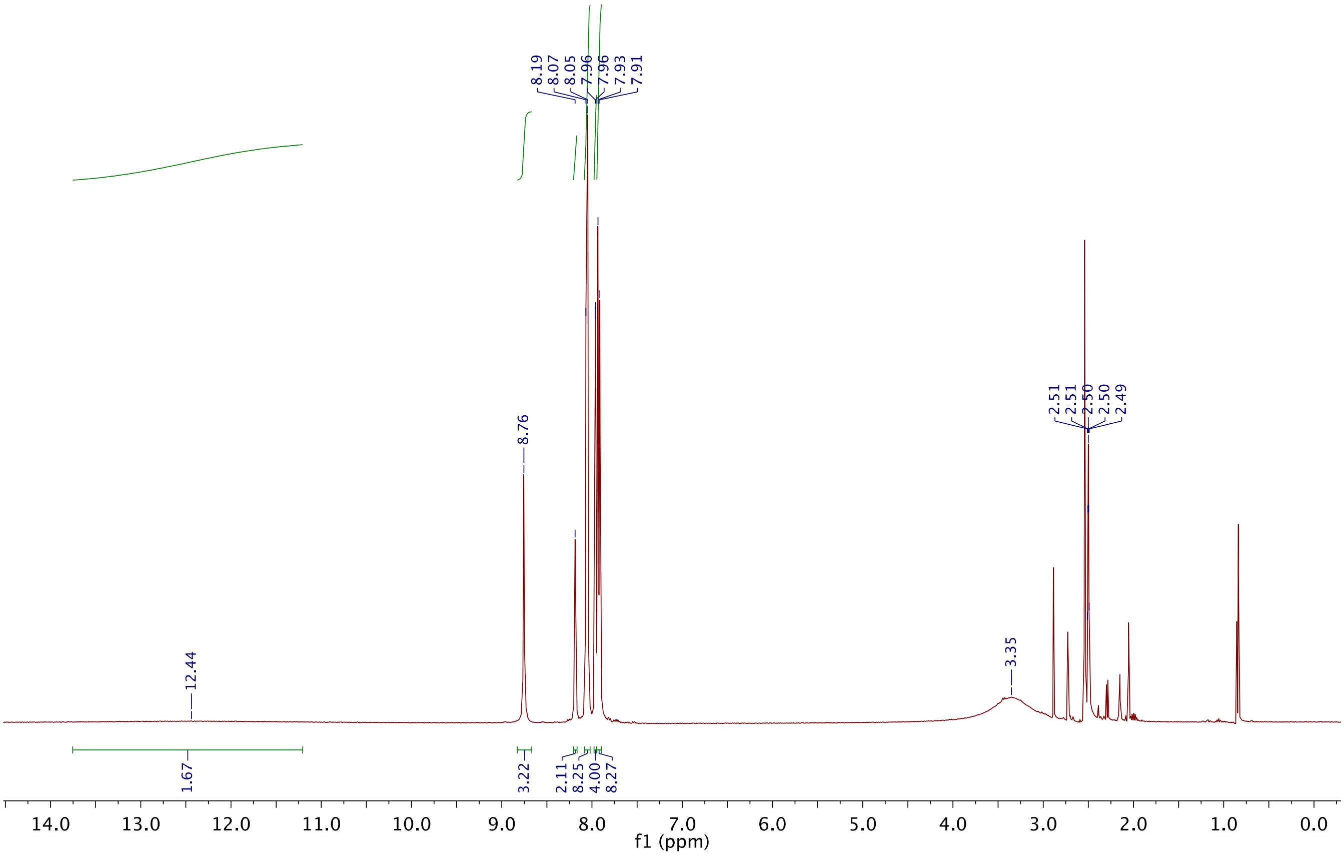

Figure S4: ^{1}H NMR spectra of N,N′- bis(terphenyl-4,4''-dicarboxylic acid) naphthalenediimide (400 MHz, DMSO-*d*$_6$).

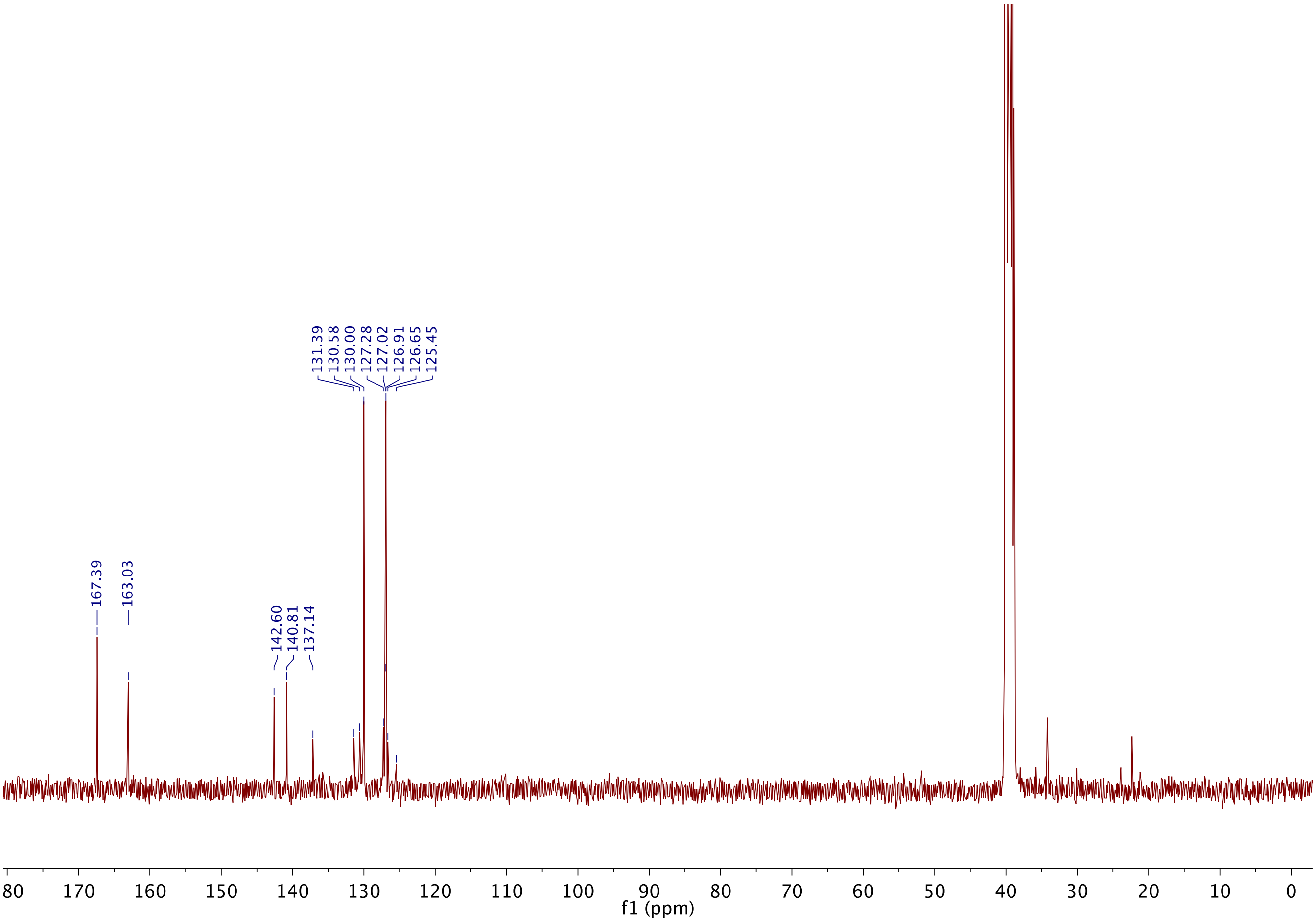

Figure S5: ^{13}C NMR spectra of N,N′- bis(terphenyl-5,5''-dicarboxylic acid) naphthalenediimide (400 MHz, DMSO-*d*$_6$).

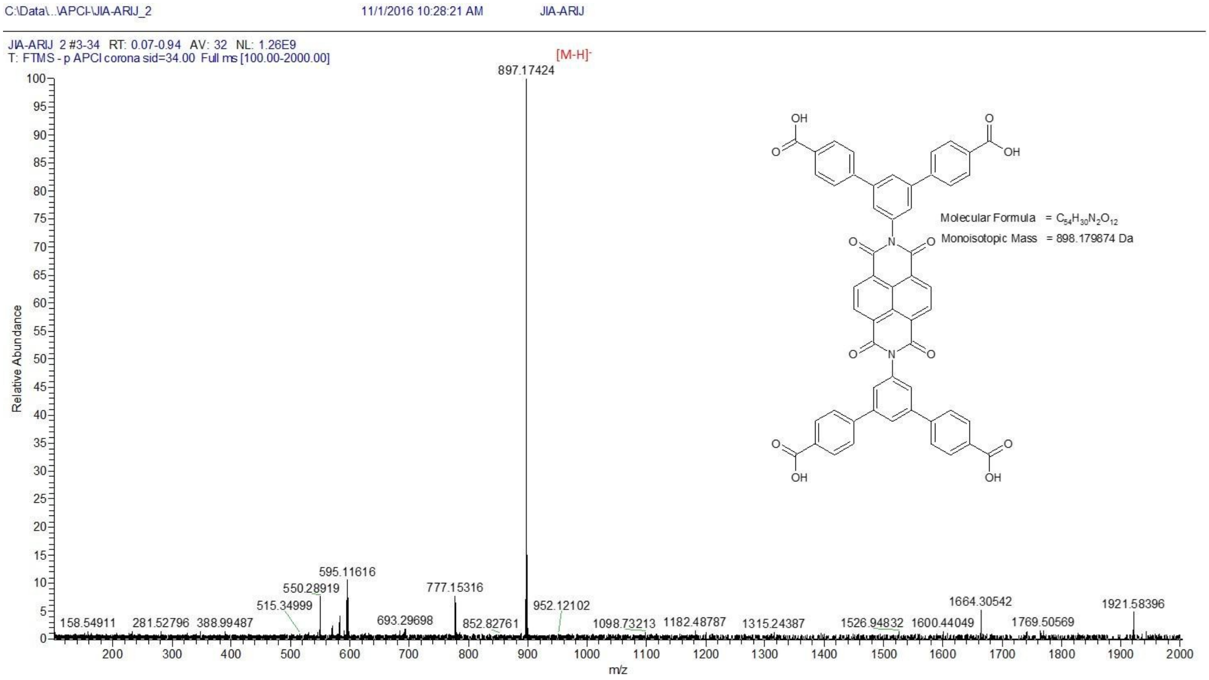

Figure S6: Mass spectra for the linker showing the exact molecular weight as calculated from the formula.

Synthesis of the Zr-NDI-scu**-MOF:** 15 mg $ZrCl_4$ (0.064 mmol) was taken into a 20 mL glass scintillation vial containing NDI-linker (6.0 mg, 0.006 mmol) and 3 mL DMF. To this 400 mg F-BzA and 0.3 mL formic acid were added. This reaction mixture was sonicated for 5 min and placed into a preheated oven at 120°C for 48 hours and cooled to room temperature yielding light yellow needle shaped crystals. Single crystals of the MOFs were collected and washed with DMF. The crystals were stored in the same solvent for further application and characterizations.

Synthesis of the Zr-NDI-BPy-sco-MOF: Compound 2 was synthesized by the linker installation of Zr-NDI-**scu**-MOF with BPy (2,2'-bipyridine-5,5'-dicarboxylate) respectively through an acid and base reaction. Scheme S1 shows the chemical equation of linker installation process. Generally, Zr-NDI-**scu**-MOF (100 mg) were treated with the solution of linear linkers in DMF (0.03 M, 40 mL) at 85ºC for 24h. The materials were collected by filtration and washed with fresh DMF 3 times (yield: 96%).

S3: Single crystal XRD and crystal structure of Zr-NDI-scu**-MOF:**

SCXRD data of **1** were collected using Bruker X8 PROSPECTOR APEX2 CCD diffractometer using Cu *K*α (λ = 1.54178 Å) radiation. Indexing was performed using APEX2 (Difference Vectors method).[1] Data integration and reduction were performed using SaintPlus 8.34A.[2] Absorption correction was performed by multi-scan method implemented in SADABS.[3] Space group was determined using XPREP implemented in APEX2. Structure was solved using Direct Methods (SHELXS-2013)[4] and refined using SHELXL-2018[5] (full-matrix least-squares on F^2) contained WinGX.[6] Crystal data and refinement conditions are shown in Table S1. A full list of restraints and constraints is contained within the CIF file. A set of DFIX, SADI, FLAT and RIGU was applied on the organic ligand to make its geometry and thermal parameters reasonable. All attempts to refine peaks of residual electron density as solvent molecules were unsuccessful. The data were corrected for delocalized electron density using of the SQUEEZE procedure[7] as implemented in PLATON.[8] The total solvent-accessible void volume of 13337 Å^3 with a total electron count of 5406 was found in the unit cell.

Table S1. Crystal data and structure refinement conditions for Zr-NDI-**scu**-MOF.

Empirical formula	$C_{108}H_{68}N_4O_{40}Zr_6$
Formula weight	2608.98
Crystal system, space group	Orthorhombic, *Cmmm*
Unit cell dimensions	a = 20.7974(9) Å, b = 34.320(1) Å, c = 24.2844(9) Å
Volume	17333(1) Å^3
Z, calculated density	2, 0.500 Mg m^{-3}
F(000)	2608
Temperature (K)	100.0(1)
Radiation type, λ	Cu $K\alpha$, 1.54178 Å
Absorption coefficient	1.67 mm^{-1}
Absorption correction	Multi-scan
Max and min transmission	0.125 and 0.041
Crystal size	0.003 × 0.03 × 0.15 mm
Shape, colour	Plate, colourless
θ range for data collection	4.4–50.4°
Limiting indices	$-20 \leq h \leq 20$, $-34 \leq k \leq 21$, $-23 \leq l \leq 24$
Reflection collected / unique / observed with $I > 2s(I)$	22259 / 4917 (R_{int} = 0.053) / 3700
Completeness to θ_{max} = 50.4°	99.4 %
Refinement method	Full-matrix least-squares on F^2
Data / restraints / parameters	4918 / 192 / 216
Final *R* indices [$I > 2\sigma(I)$]	R_1 = 0.049, wR_2 = 0.159
Final *R* indices (all data)	R_1 = 0.060, wR_2 = 0.164
Weighting scheme	$[\sigma^2(F_o^2) + (0.1134P)^2]^{-1*}$
Goodness-of-fit	1.03
Largest diff. peak and hole	0.45 and -0.61 e Å^{-3}

$^*P = (F_o^2 + 2F_c^2)/3$

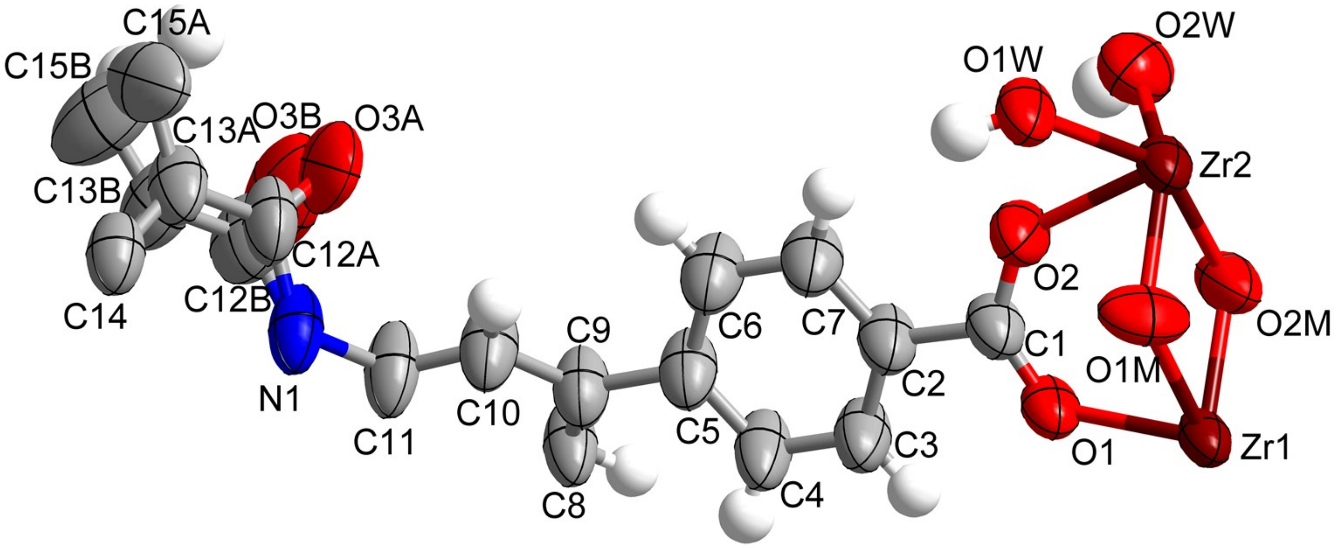

Figure S7: The asymmetric unit of Zr-NDI-**scu**-MOF crystal structure, showing thermal ellipsoids at 40% probability level and the numbering scheme.

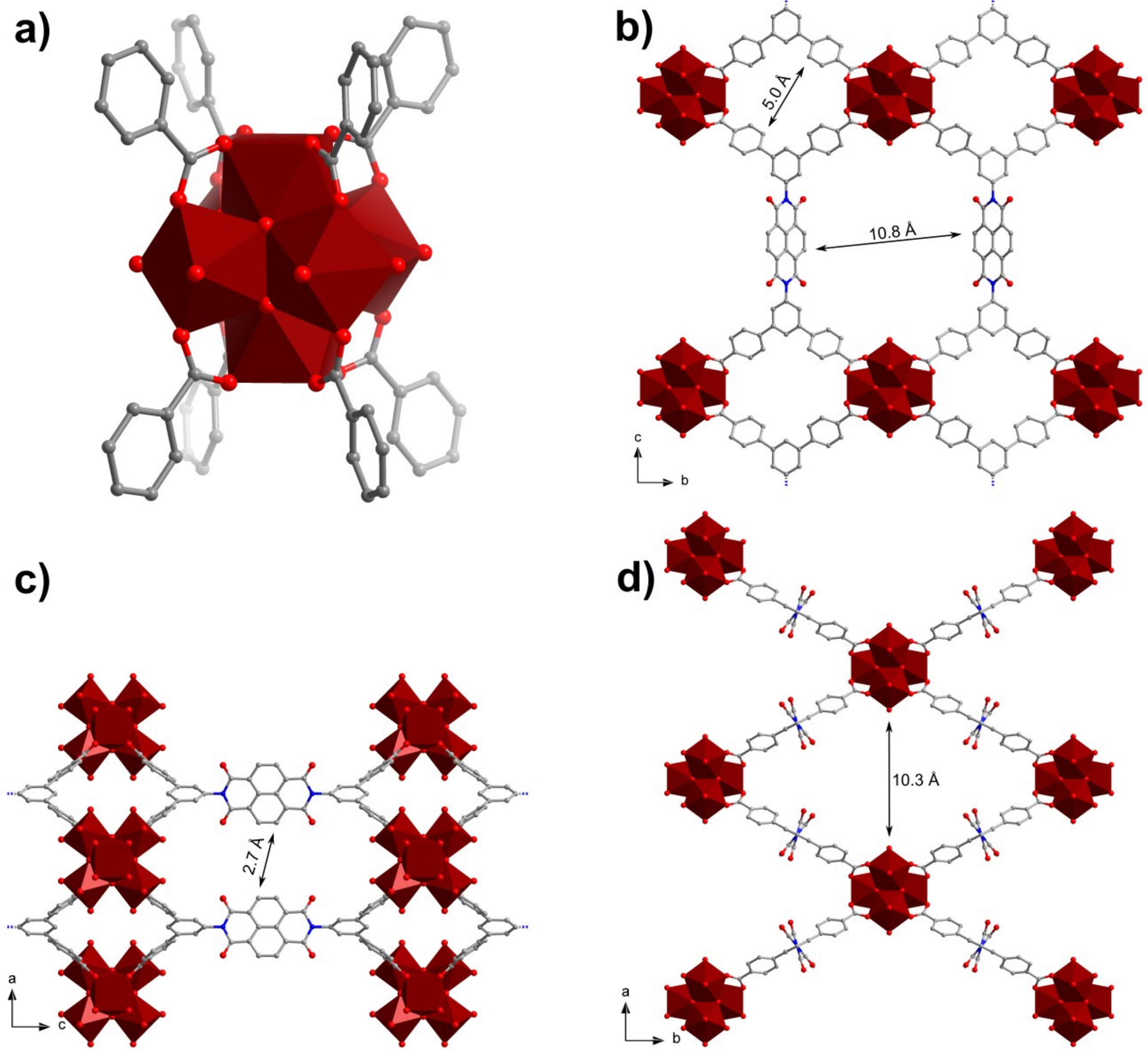

Figure S8: Crystal structure of Zr-NDI-**scu**-MOF: a) The hexanuclear Zr-cluster with 8 carboxylate form the linker. b) Two kind of apertures are observed along the crystallographic *a*-axis. c) The smallest aperture in the structure is along the crystallographic *b*-axis. d) The aperture formed by two water molecules of the opposite Zr$_6$-clusters along the crystallographic *c*-axis. Hydrogen atoms are omitted for clarity.

S4: PXRD characterization:

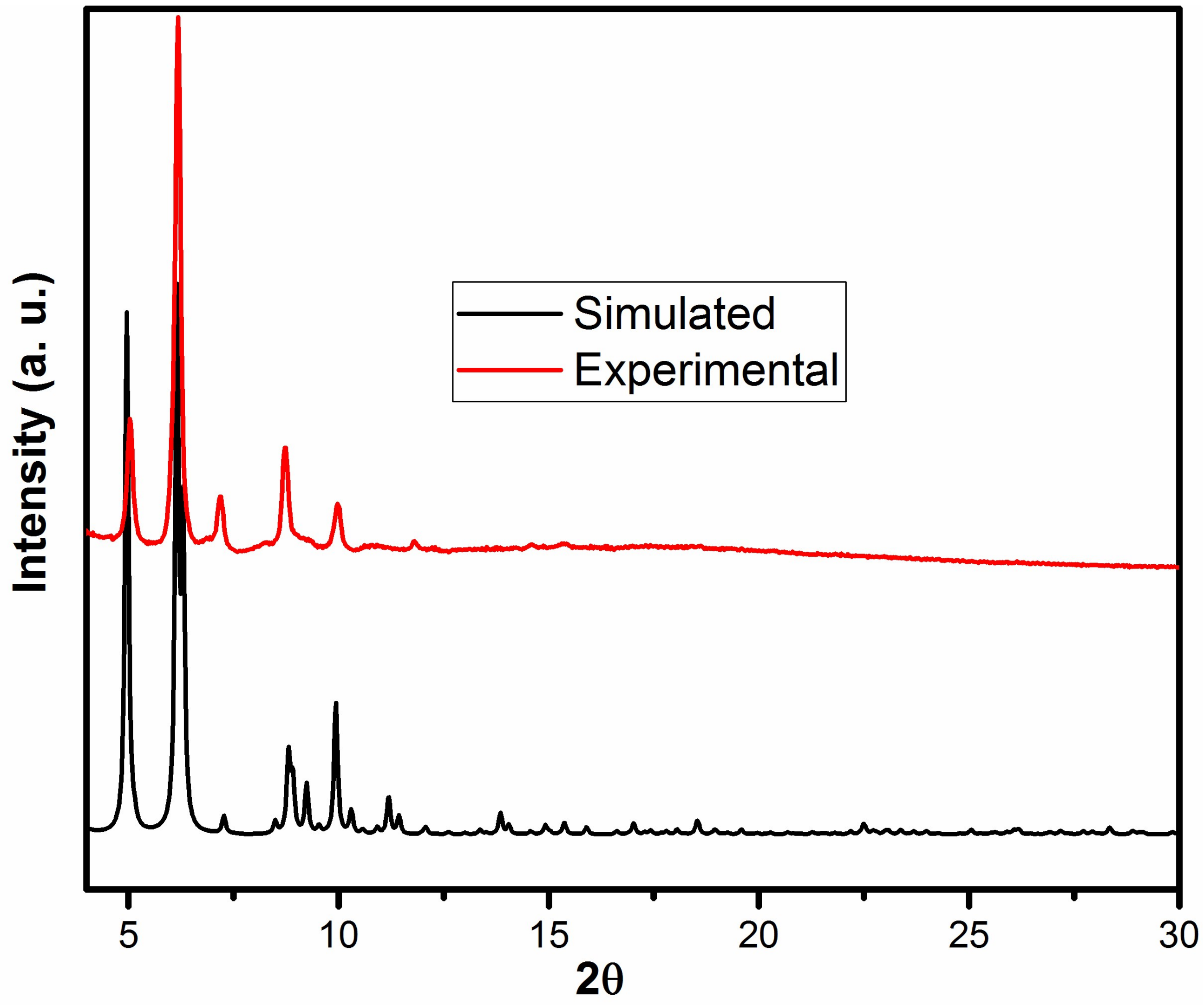

Figure S9: Comparison of PXRD pattern of experimental with simulated for Zr-NDI-**scu**-MOF.

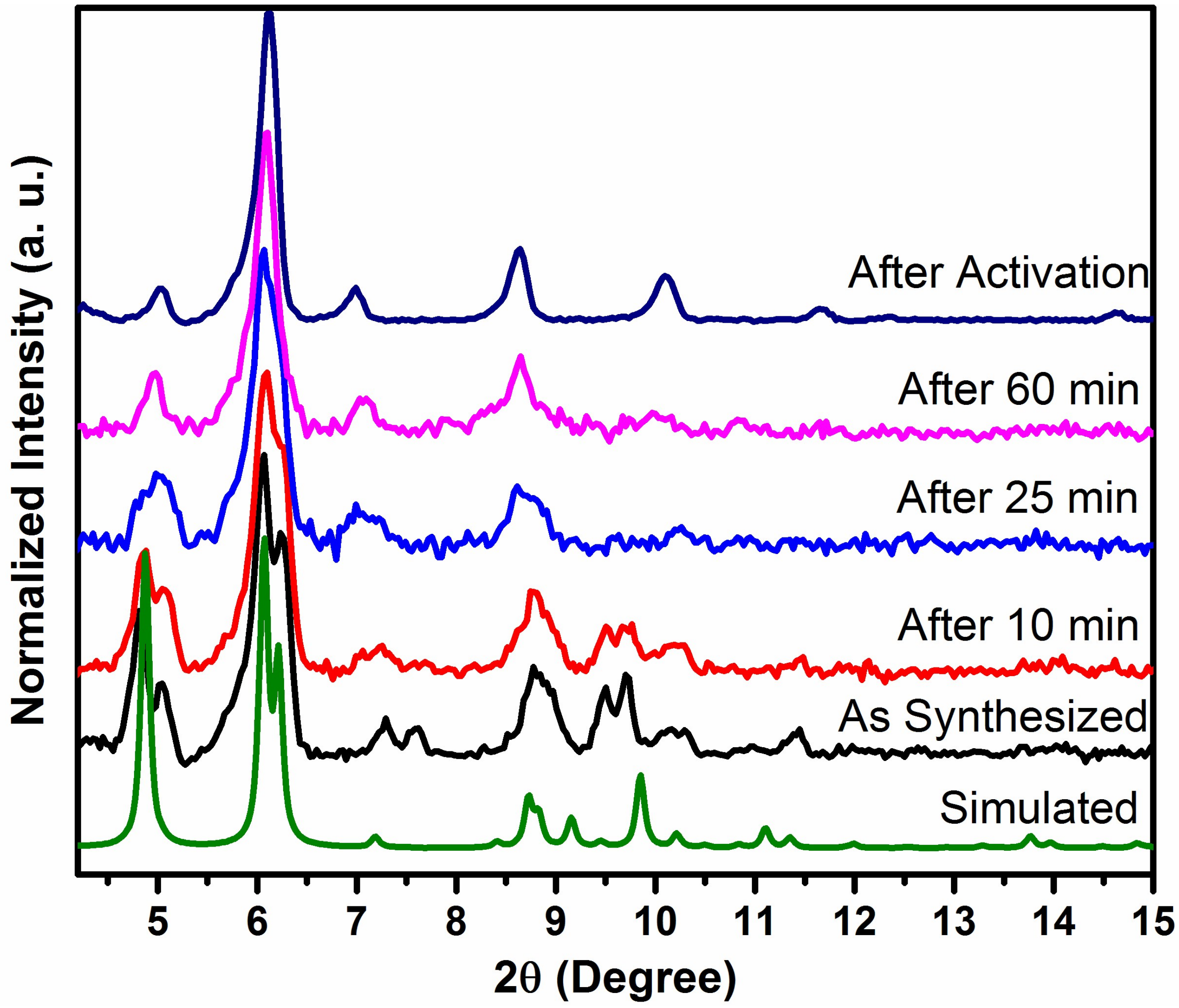

Figure S10: Time dependent PXRD pattern of for Zr-NDI-**scu**-MOF showing the peak shift with removal of the trapped solvent.

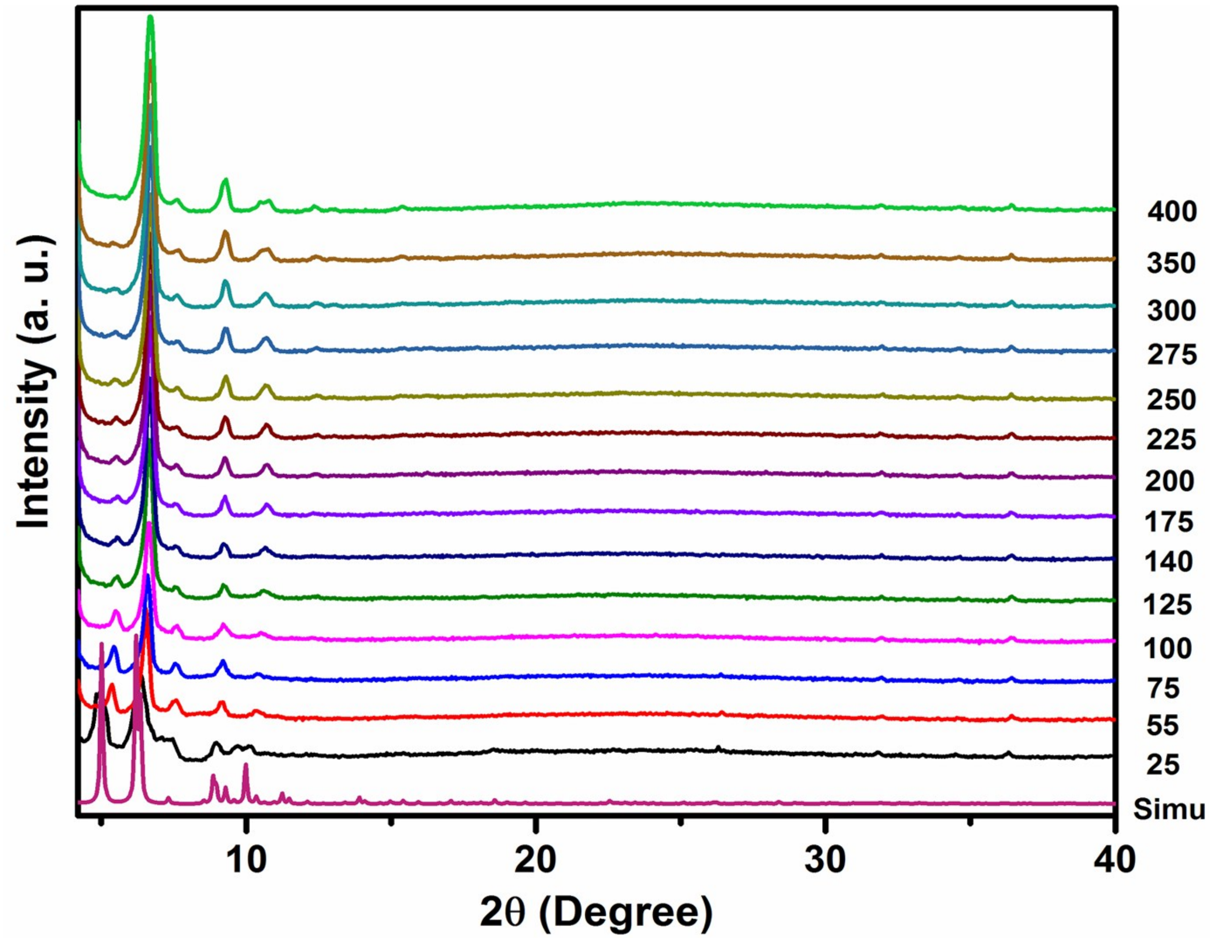

Figure S11: Variable temperature dependent PXRD pattern of for Zr-NDI-**scu**-MOF showing the thermal stability up to 400°C.

S5: BET Surface area of MOFs:

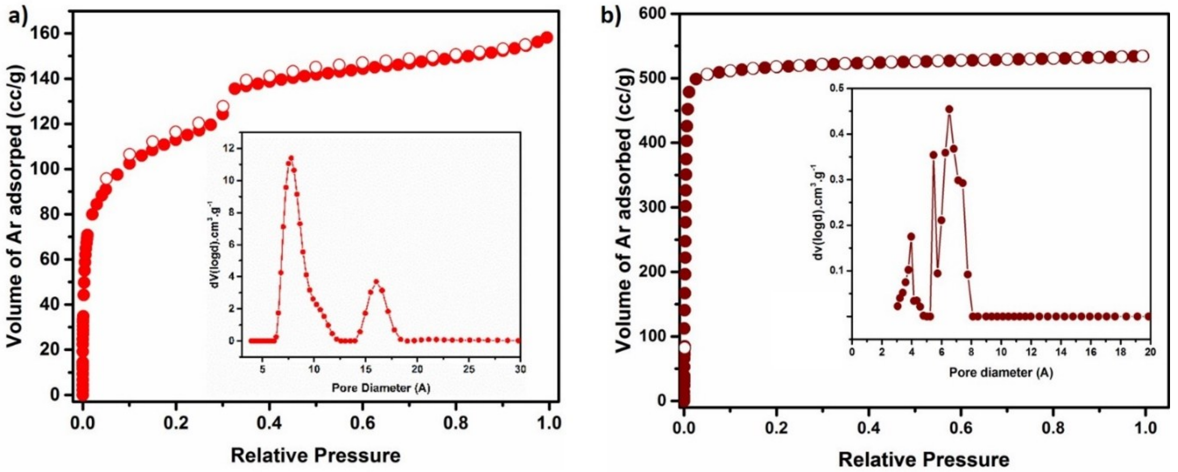

Figure S12: Ar adsorption isotherm for a) Zr-NDI-**scu**-MOF (red) and pore size distribution plot in inset and b) Zr-NDI-BPy-**sco**-MOF (brown), Pore size distribution in inset.

S6: Electrochemical measurements:

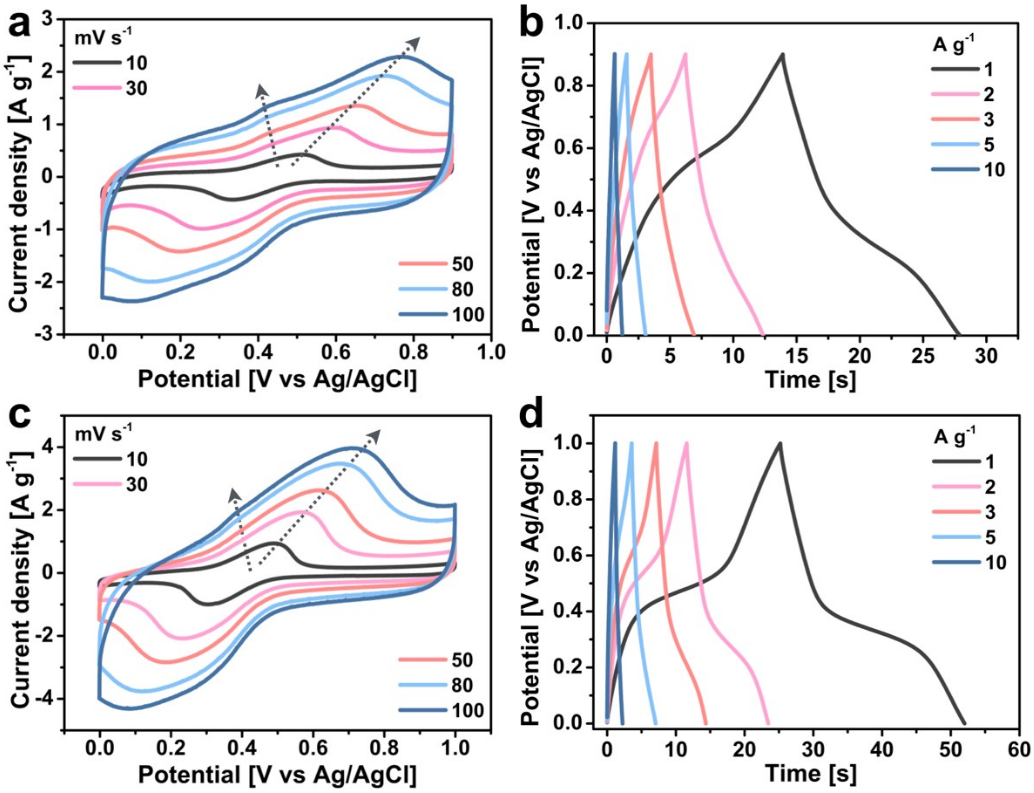

Figure S13: (a,c,) CV and (b,d,) CD curves recorded at different scan rates and current densities, respectively for (a,b) Zr-NDI-**scu**-MOF, (c,d) Zr-NDI-BPy-**sco**-MOF in three-electrode measurements using 1 M H_2SO_4 as electrolyte.

S7: Derivation of the sco net:

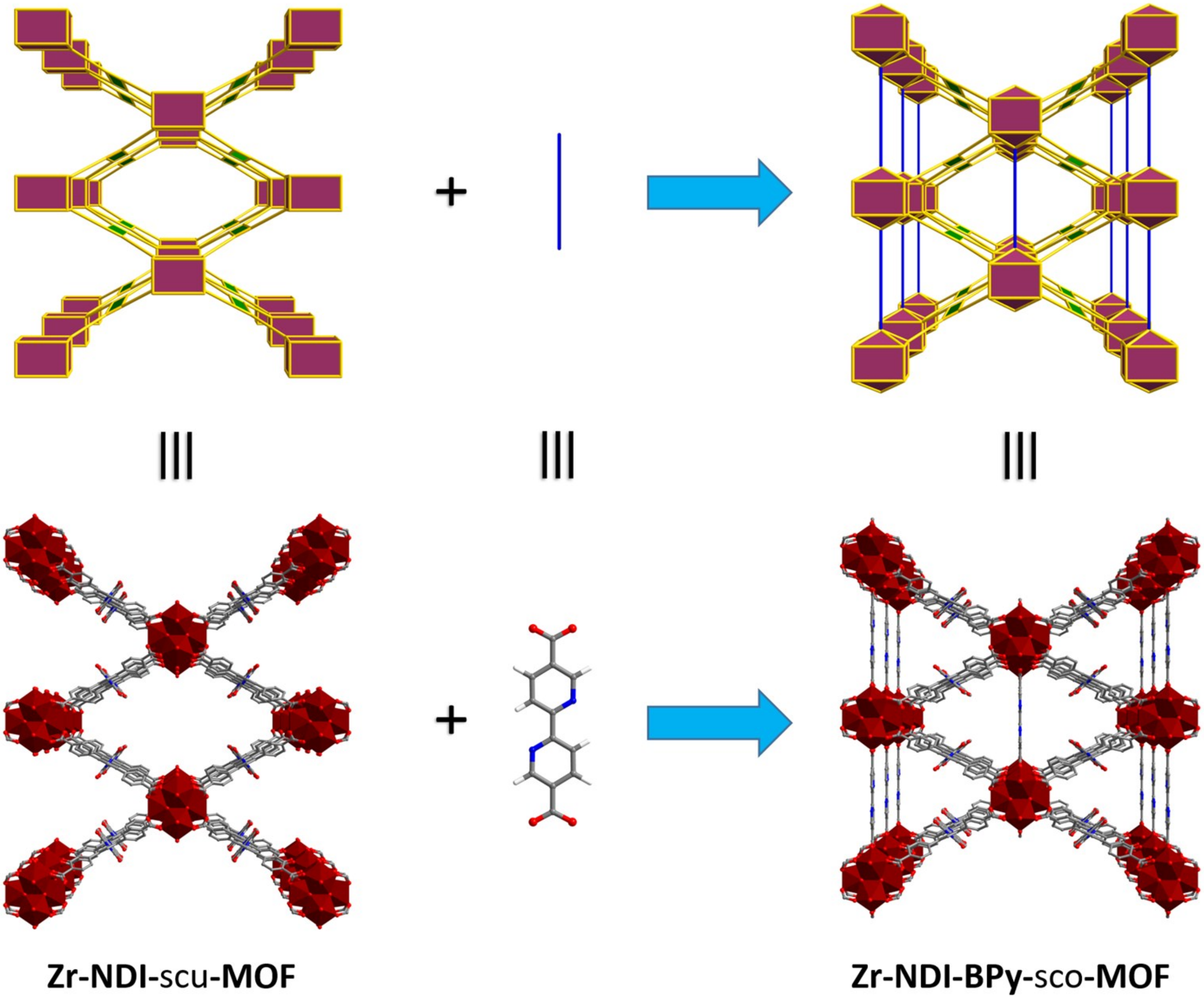

Figure S14: Derivation of the **sco** net from the **scu** net by insertion of the ditopic spacer shown in the augmented form (top) and structural representation of this process as Zr-NDI-**scu**-MOF modification *via* 2,2´-Bipyridine-5,5´-dicarboxylic acid (BPy) installation resulting in Zr-NDI-BPy-**sco**-MOF (bottom).

Geometry optimization procedure based on molecular mechanics calculations was employed for structural simulation of the Zr-NDI-BPy-**sco**-MOF. Calculations were performed with the Materials Studio, Forcite module.[9] Universal Force Field (UFF)[10] was employed for the bonded and non-bonded interactions, apart from Coulomb interactions. Partial atomic charges were calculated using Qeq approach[11] for each geometry optimization run. The optimization technique is a modified version of procedure developed by R. Snurr and A.O. Yazaydın.[12] The LJ cutoff distance of 18.5 Å was used for geometry optimization calculations. The Ewald sum technique was employed to calculate the electrostatic interactions

S8: NMR measurements of Zr-BTD-NDI-BPy-MOF:

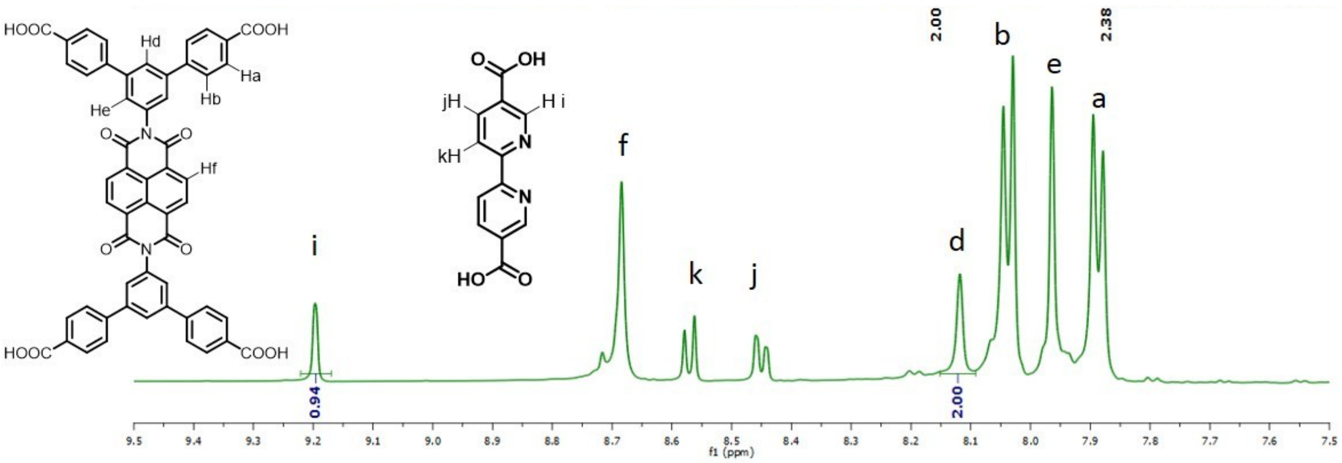

Figure S15: ^{1}H NMR (400 mHz, DMSO-d_6) spectra for the pillar installed MOFs. For ^{1}H NMR analysis of Zr-NDI-BPy-**sco**-MOF, the sample (around 5 mg) were digested by 12N HCl aqueous solution and dried in a 100°C oven. The solid was dissolved in about 0.5 mL DMSO-d_6.

S9: PXRD comparison:

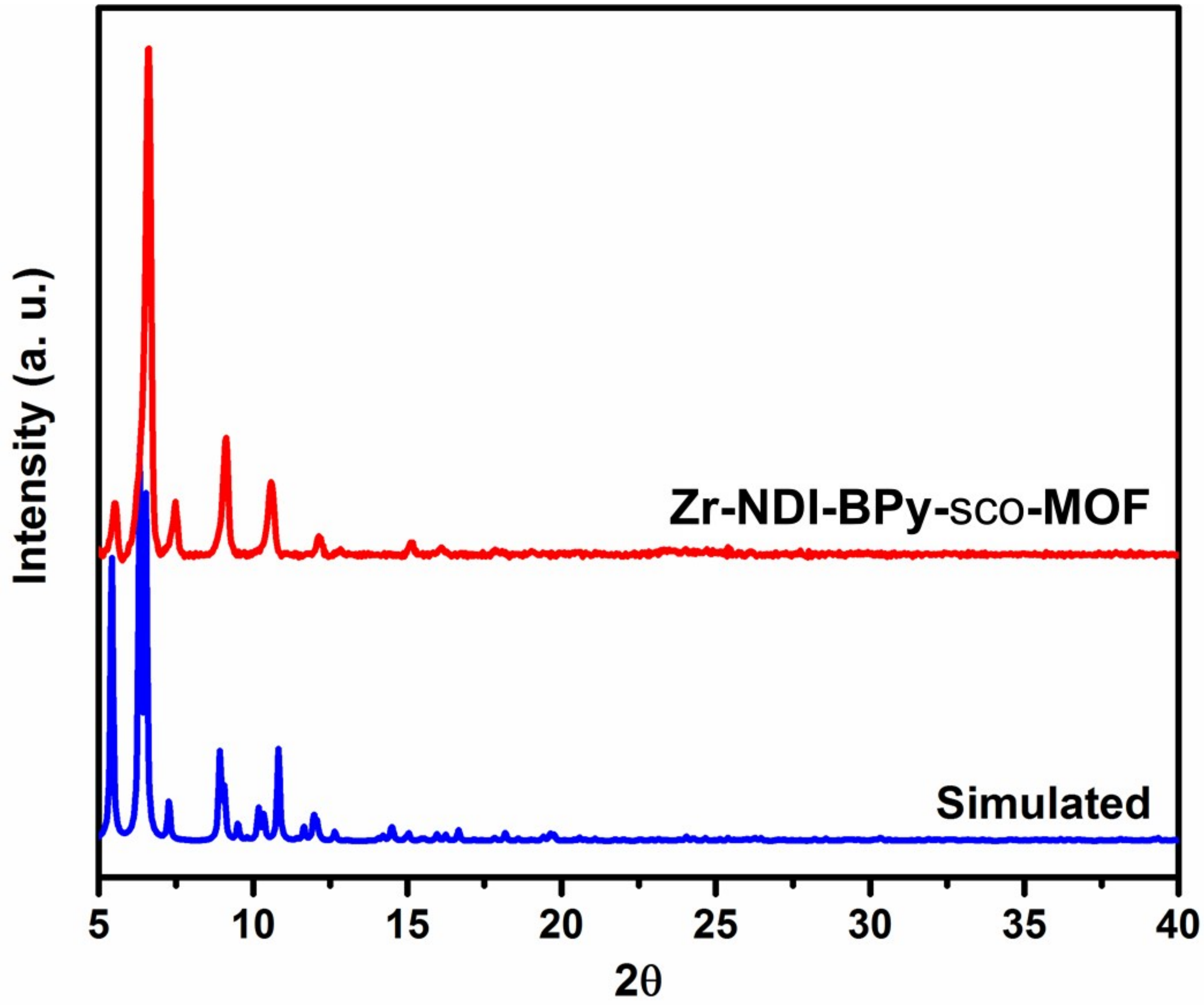

Figure S16: Comparison of the PXRD pattern of bulk Zr-NDI-BPy-**sco**-MOF crystal (red) with their simulated pattern (blue).

S10: FT-IR spectroscopy characterization:

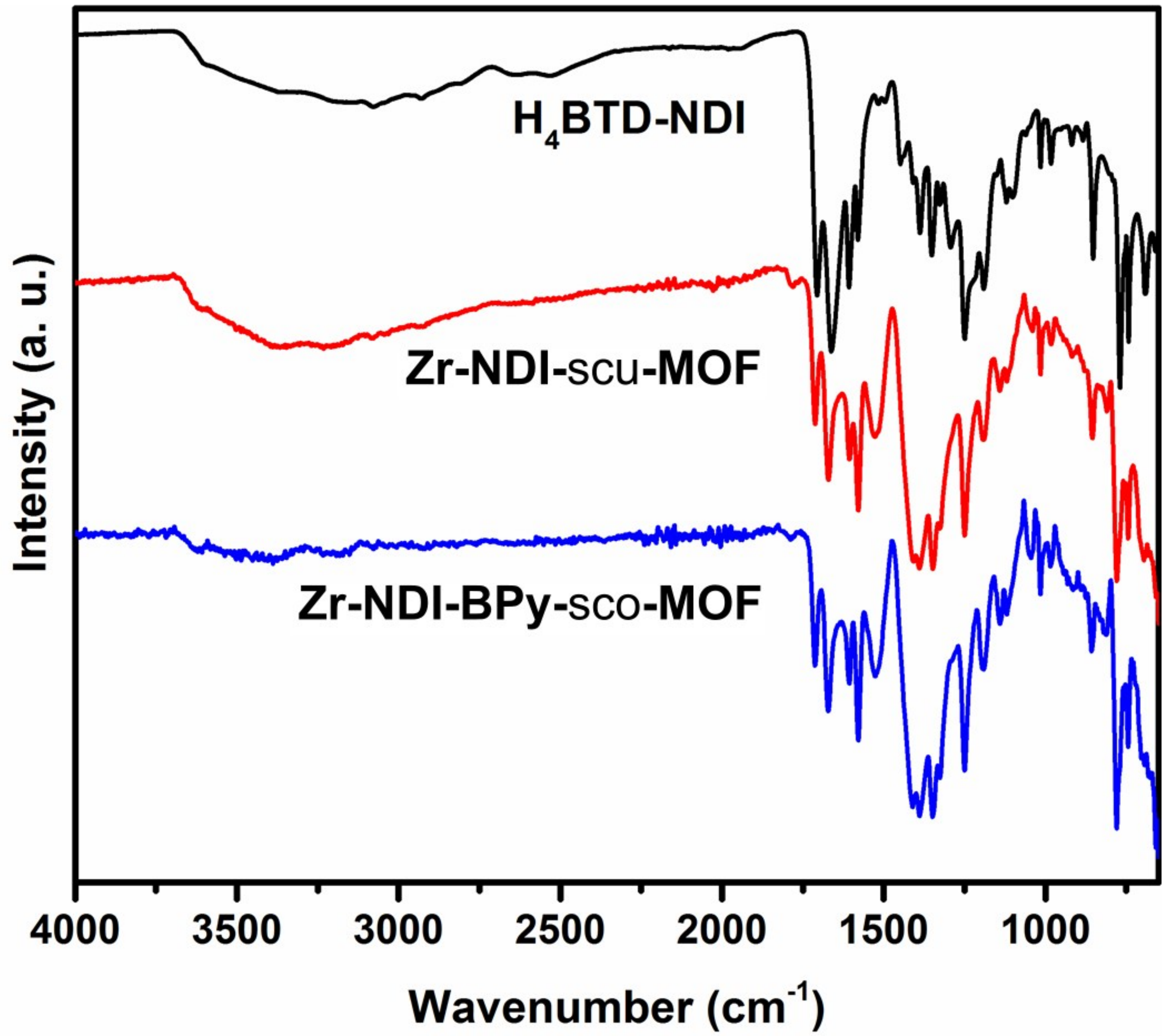

Figure S17: Comparison of FT-IR spectra of the linker and all other MOFs.

S11: TG analyses:

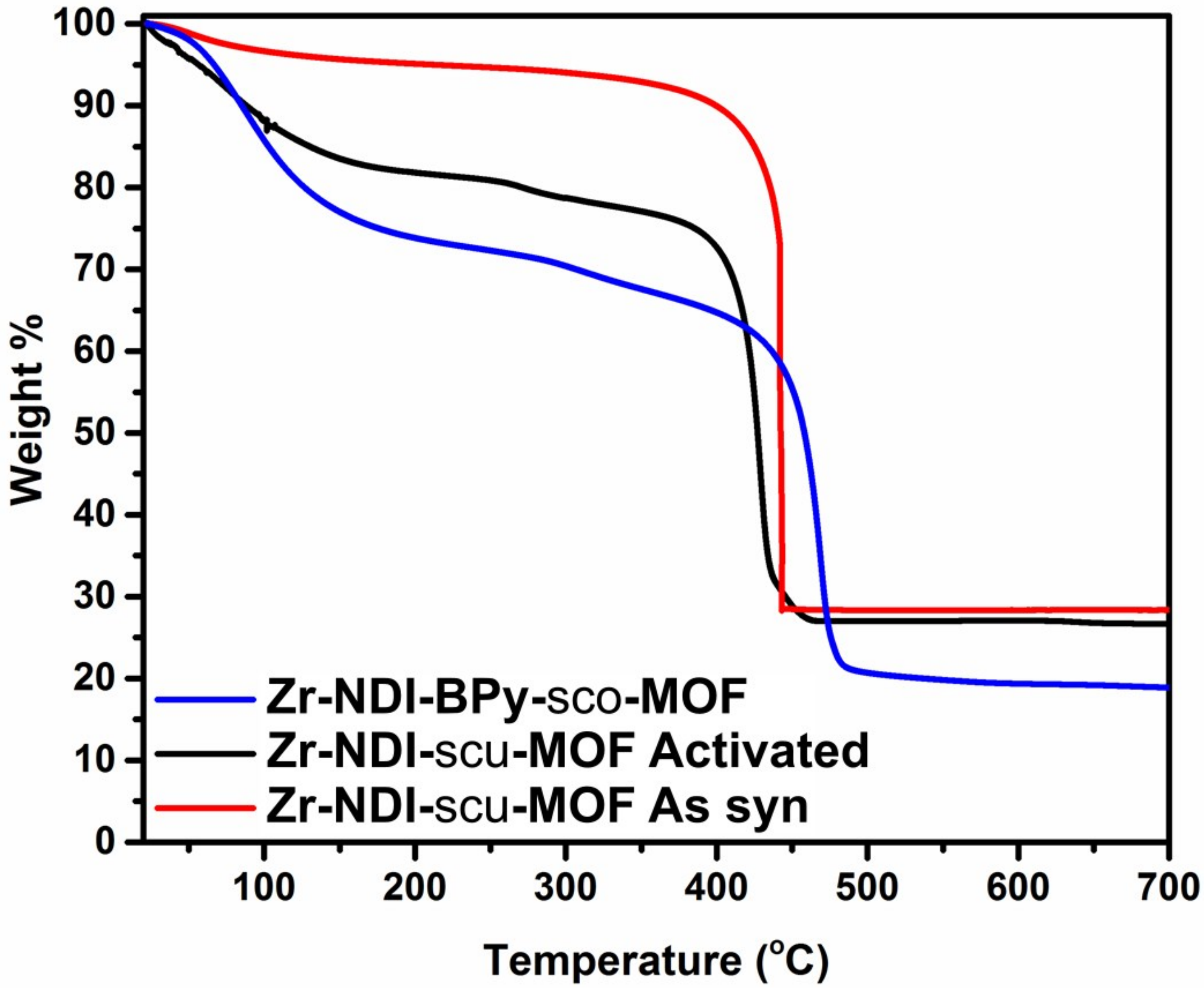

Figure S18: TGA plots of the synthesized MOFs showing their thermal stability.

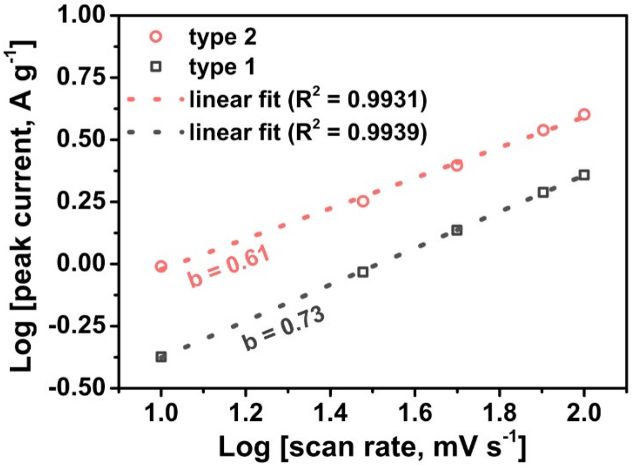

Figure S19. Peak currents of Zr-NDI-**scu**-MOF and Zr-NDI-BPy-**sco**-MOF materials against scan rate for the determination of *b* values.

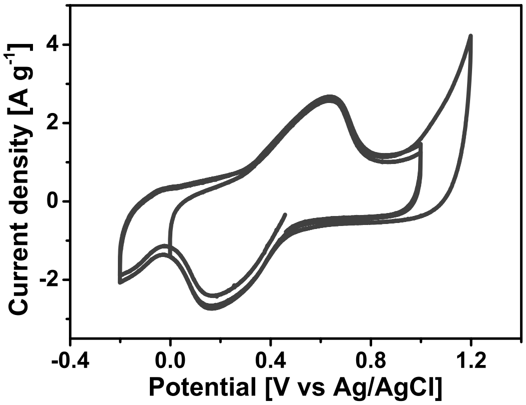

Figure S20. CV curves showing that the potential window of Zr-NDI-BPy-**sco**-MOF could be extended to 1.0 V, which indicates that the oxygen evolution reaction was restricted to some degree compared to Zr-NDI-**scu**-MOF.

S12: SEM characterization:

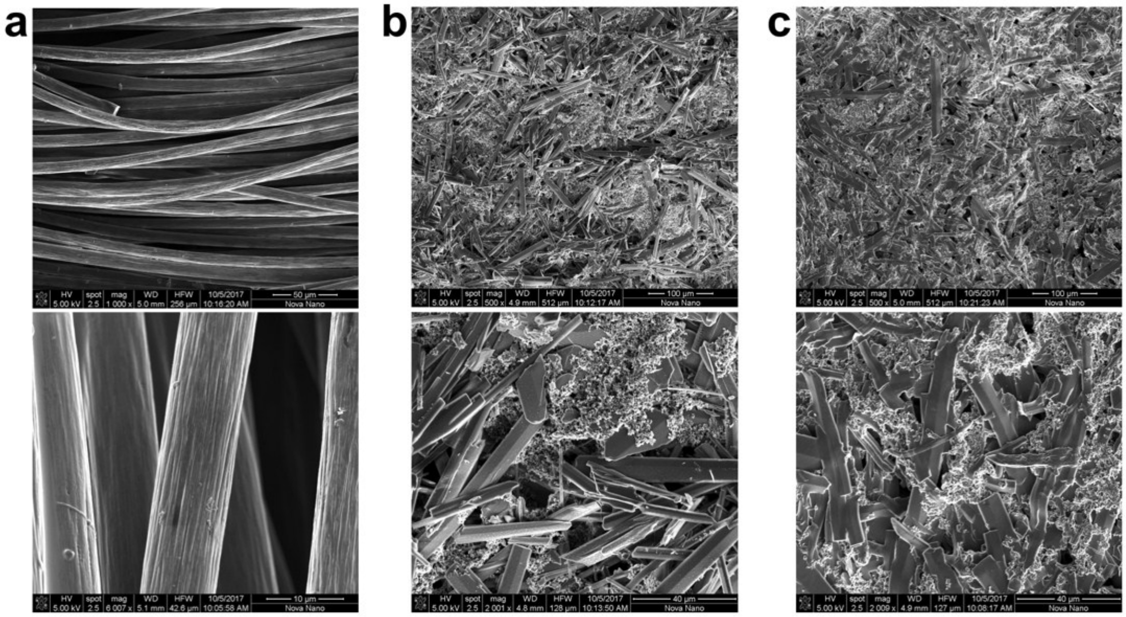

Figure S21. Low (top panel) and high-magnification (bottom panel) SEM images of (a) carbon cloth (CC) electrode, (e) Zr-NDI-BPy-**sco**-MOF on CC electrode, and (c) MOF electrode after cycling.

Table S2. Comparison of the Zr-NDI-BPy-**sco**-MOF and other reported MOFs (data from *ACS Nano*, **2014**, *8*, 7451).

Material	Areal capacitance (mF cm^{-2})	Electrolyte	Voltage window (V)	Cycle number	Capacity retention (%)
Zr-NDI-BPy-**sco**-MOF	5.48	1 M H_2SO_4	0.0-1.0	10,000	99.9
nMTV-MOF-5-AE	0.913	1 M $(C_2H_5)_4NBF_4$	0.0-2.5	3,000	80
nM7M-MOF-74	1.155	1 M $(C_2H_5)_4NBF_4$	0.0-2.5	300	80
nHKUST-1	2.33	1 M $(C_2H_5)_4NBF_4$	0.0-2.5	6,000	80
nMOF-177	0.713	1 M $(C_2H_5)_4NBF_4$	0.0-2.5	4,000	80
nZIF-8	0.268	1 M $(C_2H_5)_4NBF_4$	0.0-2.5	2,500	80
nUiO-66	1.945	1 M $(C_2H_5)_4NBF_4$	0.0-2.5	7,000	80
nMOF-867	5.085	1 M $(C_2H_5)_4NBF_4$	0.0-2.5	10,000	80
activated carbon	0.788	1 M $(C_2H_5)_4NBF_4$	0.0-2.5	10,000	80
graphene	0.515	1 M $(C_2H_5)_4NBF_4$	0.0-2.5	10,000	80

S13: References

1. Bruker-AXS (2014). APEX2. Version 2014.11-0. Madison, Wisconsin, USA.
2. Bruker-AXS (2013). SAINT. Version 8.34A. Madison, Wisconsin, USA.
3. Krause, L., Herbst-Irmer, R., Sheldrick, G. M. & Stalke, D. (2015). J. Appl. Cryst. 48, 3-10.
4. Sheldrick, G. M. (2018). SHELXS. Version 2018/3. Georg-August-Universität Göttingen, Göttingen, Germany.
5. Sheldrick, G. M. Acta Cryst. (2015) C71, 3-8.
6. Farrugia, L. J. J. Appl. Cryst. (2012), 45, 849-854.
7. Spek, A. L. Acta Cryst. (2015), C71, 9-18.
8. Spek, A. L. Acta Cryst. (2009), D65, 148-155.
9. Materials Studio 7.0, Accelrys Software Inc., San Diego, CA 92121, USA.
10. Rappe, A. K.; Casewit, C. J.; Colwell, K. S.; Goddard III, W. A.; Skid, W. M. J. Am. Chem. Soc. 1992, 114, 10024−10035.
11. Rappe, A. K.; Goddard III, W. A. J. Phys. Chem. 1991, 95, 3358−3363.
12. Farha, O. K.; Özgür Yazaydın, A.; Eryazici, I.; Malliakas, C. D.; Hauser, B. G.; Kanatzidis, M. G.; Nguyen, S. T.; Snurr, R. Q.; Hupp, J. T. Nature Chem. 2010, 2, 944-948.